






Article

Experiments on a Real-Time Energy Management System for Islanded Prosumer Microgrids

Carlos A. Macana ^{1,*} , Hemanshu R. Pota ¹ , Quanyan Zhu ² , Josep M. Guerrero ³  and Juan C. Vasquez ³ 

¹ School of Engineering and Information Technology, University of New South Wales, Canberra 2612, Australia

² Department of Electrical and Computer Engineering, Tandon School of Engineering, New York University, Brooklyn, NY 11201, USA

³ Institute of Energy Technology, Aalborg University, 9100 Aalborg, Denmark

* Correspondence: carlos.macana@student.adfa.edu.au

Received: 4 July 2019; Accepted: 19 August 2019; Published: 23 August 2019



Abstract: This paper presents an experimental demonstration of a novel real-time Energy Management System (EMS) for inverter-based microgrids to achieve optimal economic operation using a simple dynamic algorithm without offline optimization process requirements. The dynamic algorithm solves the economic dispatch problem offering an adequate stability performance and an optimal power reference tracking under sudden load and generation changes. Convergence, optimality and frequency regulation properties of the real-time EMS are shown, and the effectiveness and compatibility with inner and primary controllers are validated in experiments, showing better performance on optimal power tracking and frequency regulation than conventional droop control power sharing techniques.

Keywords: microgrids; power electronics; power sharing control; energy management systems; cyber-physical systems

1. Introduction

The successful implementation of policies to stimulate the integration of Renewable Energy Sources (RESs) and the decreasing cost of Battery Energy Storage Systems (BESSs) [1] have generated an important role of new energy system components including the concepts of “prosumer” [2] and “microgrid” [3]. A prosumer is defined as a consumer that has capacity to generate energy [4]. On the other hand, a microgrid is defined as a cluster of Inverter based Distributed Generators (IDGs) and controllable loads, which are interconnected and can operate autonomously in grid-connected or island mode [3,5]. The microgrid concept has been proposed as a systematic approach to deal with the distribution grid challenges, and this is considered an essential component towards the new Smart Grids [6]. Integrating the concepts of microgrid and prosumer, a Prosumer Microgrid (PMG) can be defined as a cluster of prosumers and costumers with capacities of energy generation, load control, and autonomous operation. The PMGs potentially will be able to configure new types of local energy markets and energy systems [2]. In this context, the efficiency is a main objective for planning, design and operation of the PMG, and the operation cost minimization needs to be considered as an essential control task [7].

Traditionally, the power sharing control for microgrids commonly defines the proportional power sharing as the main goal [8,9]. The conventional control approach to deal with this requirement is known as the droop control technique. Although this approach can achieve accurate active proportional power sharing, which is a basic safety operation requirement (i.e., each IDG does not exceed maximum

generation restrictions), this approach does not include any economic operation criteria. In this paper, an alternative power sharing operation strategy is proposed, which holds both maximum capacity generation requirements and optimal economic operation in real-time. In this way, we study the Economic Dispatch Problem (EDP) in a PMG. Specifically, a coordinator agent called Microgrid Central Controller (MGCC) [10–12] aims to minimize the total energy cost required to supply the total load demand in the PMG subject to restrictions on the power generation of the IDG. Traditionally, this task is performed for conventional energy generation systems by an offline process on the tertiary control level and using long time scales (order of tens of minutes and hours) [13]. However, if the economic dispatch process is not performed in real-time in the PMG scenario, it could result in sub-optimal operation points, which do not minimize the total energy cost, owing to the random changes in the load demand and the RES generation [14]. In this way, based on the assumption that instantaneous active power measurements are available in each local controller, which is a common characteristic in most of the primary control strategies of the EDP [15], a novel real-time energy management strategy is proposed to deal with the economical operation of a PMG. A general framework for a PMG is presented in Figure 1, where the communication architecture between primary controllers of each IDG and the MGCC is shown.

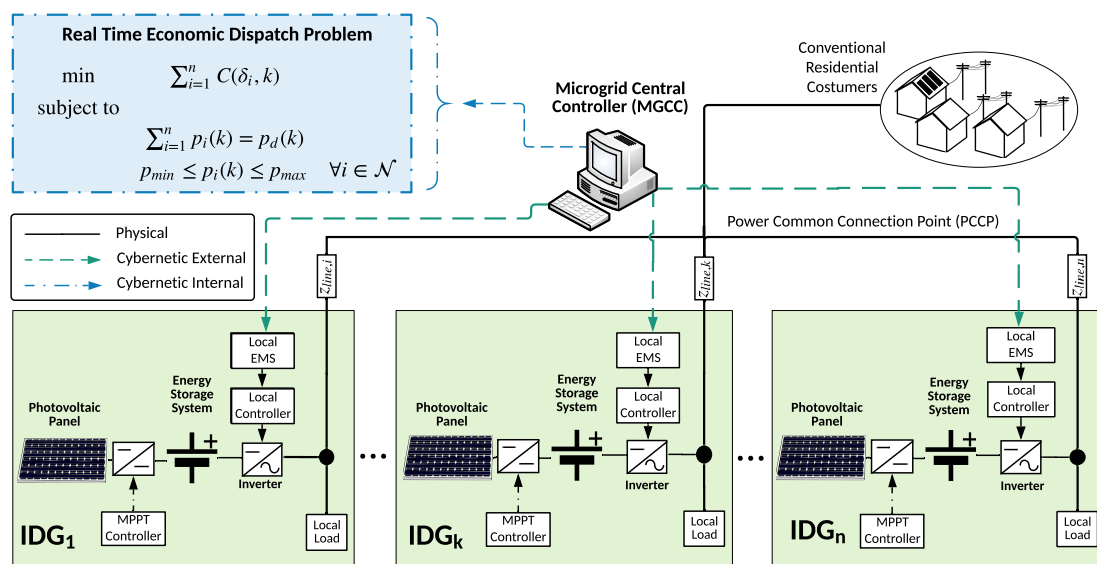


Figure 1. Prosumer Microgrid Architecture and the Real-time Economic Dispatch Problem.

The main contribution of this paper is an experimental proof of concept of a novel optimal real-time strategy to solve the EDP for an islanded PMG. Unlike most of the previous approaches, the EDP is solved using real-time data of the measured instantaneous output active power of the IDGs. In this way, a dynamic algorithm with low implementation complexity guarantees fast convergence, optimality and good frequency regulation performance. This real-time approach eliminates the requirements of offline optimization process of several strategies proposed previously [7,16,17] and leads to a proper frequency regulation performance. In addition, the results of the experimental validation of the strategy are presented, which differentiates this paper from most of related theoretical works reported in the literature [12,14,16–18].

1.1. Related Work

Previous Energy Management System (EMS) proposals for microgrids require accurate knowledge of the total load demand and available RES generation in each optimization period, where typically complex load forecast and estimation algorithms are used [7,16,17]. These offline dispatch strategies are highly dependent on accurate forecast of generation and load demand [14,16,17]. However, in a PMG scenario with high penetration of RESs, IDGs and uncontrollable loads, the forecasting

inaccuracy can lead to a non-optimal power allocation owing to the random characteristics of the energy generation and demand [14]. Luna et al. reported experimental validations of online energy management strategies in [7], which require forecasting data and a specialized optimization software to solve the optimization problem. Although the strategies show good performance under online operation, the forecast and specialized optimization software requirements lead to high computation burden and expensive communication requirements [16]. On the other hand, Macana et al. [14] have proposed a centralized EMS to solve the EDP in real-time in a PMG, operating in grid connected mode, and assuming that the injected power of each distributed generator is sent to the MGCC. This strategy computes the power references for each IDG based on a dynamic algorithm and has shown good performance; however, the islanded scenario, which is an essential operation mode of a PMG, has not been addressed, and an experimental validation has not been included. In a similar way, most of the proposed strategies to cope with the EDP for microgrids have been only tested in simulation studies and have not reported experimental validations [12,14,16–18]. A complete literature review of EMS for microgrids can be found in [16].

In this work, we address the EDP in the islanded operation mode, considering a complete control design including the inner and primary control architecture, which follows standard design methodologies previously reported in [19,20]. The optimality and convergence analysis in Section 4 mainly follow the work [14], which is complemented in this paper with a novel analysis of the frequency regulation property of the real-time EMS strategy. As a main advantage of the proposed approach, when using this control scheme a secondary control level for frequency regulation is not required because the EMS performs an implicit frequency regulation task. This is a consequence of the optimal power allocation and could reduce the complexity and cost of the microgrid control implementation.

1.2. Notation

The set of real numbers is denoted as \mathbb{R} , and the non-negative real numbers as $\mathbb{R}_{\geq 0}$, \mathbb{N} denotes the set of natural numbers, \mathbb{C} the set of complex numbers, and $\mathbb{S} := [0, 2\pi)$. Bold style denotes column vectors (e.g., \mathbf{x}), and scalars are notated by non-bold style (e.g., a). $T_{abc \rightarrow \alpha\beta}$ and $T_{\alpha\beta \rightarrow abc}$ denote the direct and inverse Clarke's Transformation respectively [21]. The set of IDGs in the PMG is denoted as $\mathcal{N} = \{1, \dots, n\}$, where $n \in \mathbb{N}$.

1.3. Organization of the Paper

The remainder of this paper is organized as follows. Section 2 introduces an overview of the PMG system and the real-time economic dispatch problem. The proposed real-time EMS is presented in Section 3, which is followed by the presentation of the convergence, optimality and frequency regulation characteristics of the strategy in Section 4. Experimental study cases, results and discussion are given in Section 5 including a detailed description of the IDG inner and primary controllers. Finally, Section 6 provides some final conclusions and directions for future work.

2. The Prosumer Microgrid System and the Economic Dispatch Problem

An islanded PMG scenario is shown in Figure 1. The PMG consists of n prosumers, which have installed two DC-AC converters. One of the converters operates as a non-dispatchable generator, based on a Photovoltaic System (PV) with a Maximum Power Point Tracking (MPPT). The second converter integrates a dispatchable unit that uses a BESS as the power source. It is assumed that the prosumers of the PMG are willing to cooperate and have as objective to maximize the total economic benefit. The customers without storage capacity are considered as an external load of the PMG, which could be negative (see conventional residential costumers in Figure 1).

The connection of most RESs to a microgrid requires intelligent power electronics interfaces consisting of DC-AC converters (also known as “inverters”). In grid connected operation, the IDG traditionally operate as current-source inverters to inject power to the grid, and in autonomous mode (also called island operation) at least one of the IDG operates as voltage source inverter,

where the generators need to keep the system voltage amplitude and frequency according to quality standards [20]. In the scenario presented in Figure 1, the IDGs have a BESS connected to an inverter, regulating frequency and voltage on the connection point. On the other hand, it is assumed that each BESS is charged by roof PV panels with MPPT controllers and connected with battery charge control devices. The dispatchable BESS must guarantee the energy quality and availability. In this way, the frequency and voltage references must be strictly regulated and the load demand and generation must be balanced under sudden load or generation changes. Additionally, to guarantee an optimal operation an EMS needs to be implemented in order to minimize the required total generation energy cost for supplying the total load demand.

2.1. The Real Time Economic Dispatch Problem

An EMS aims to optimize the MG operation solving the EDP, which can be described by:

$$\begin{aligned} \min_{p_1, \dots, p_n} \quad & \sum_{i \in \mathcal{N}} C_i(p_i) \\ \text{subject to} \quad & \sum_{i \in \mathcal{N}} p_i = p_d, \quad \forall i \in \mathcal{N} \\ & p_{\min, i} \leq p_i \leq p_{\max, i}, \quad \forall i \in \mathcal{N} \end{aligned} \quad (1)$$

where p_d is the total load demand in the MG, p_i is the generated power of the i th IDG, $\mathcal{N} = \{1, \dots, n\}$ is the set of prosumers in the PMG, and $C_i(p_i)$ is the cost function of each IDG.

Assumption 1. The energy cost function of each IDG is assumed as a general quadratic function given by [17]:

$$C_i(p_i) = \alpha_i + \beta_i p_i + \gamma_i p_i^2 \quad (2)$$

where $\alpha_i \in \mathbb{R}_{>0}$, $\beta_i \in \mathbb{R}_{>0}$ and $\gamma_i \in \mathbb{R}_{>0}$.

2.2. Solution of the Relaxed EDP

Firstly, we consider the relaxed EDP, which consists in neglecting the inequality constraints of the EDP. This problem is formulated using the Lagrangian as [18]:

$$F(p_i, \lambda) = \sum_{i \in \mathcal{N}} C_i(p_i) + \lambda \left(\sum_{i \in \mathcal{N}} p_i - p_d \right) \quad (3)$$

The first-order optimality conditions are given by [22]: $\nabla_{p_i} C_i(p_i) - \lambda^* = 0$, where $\lambda^* \in \mathbb{R}$ is the Lagrangian multiplier of the equality constrain of (1). From (2) we can obtain:

$$\lambda^* = \nabla_{p_i} C_i(p_i) = \beta_i + 2\gamma_i p_i \quad (4)$$

Multiplying by $\frac{1}{2\gamma_i}$ and summing over all n on both sides of the equation, the optimal Lagrangian multiplier (λ^*) of the EDP is found as:

$$\lambda^* = \frac{\sum_{i \in \mathcal{N}} p_i + \sum_{i \in \mathcal{N}} \frac{\beta_i}{2\gamma_i}}{\sum_{i \in \mathcal{N}} \frac{1}{2\gamma_i}} \quad (5)$$

and the power references that minimize the total energy cost are given by:

$$p_{r,i}^* = \frac{\lambda^* - \beta_i}{2\gamma_i} \quad (6)$$

2.3. Solution of the EDP with Power Capacity Constrains

To solve the EDP including the power constrains, we define the sets

$$\Omega_M = \left\{ i : \left(\frac{\lambda - \beta_i}{2\gamma_i} \right) > p_{max,i} \right\} \quad (7)$$

and,

$$\Omega_m = \left\{ i : \left(\frac{\lambda - \beta_i}{2\gamma_i} \right) < p_{min,i} \right\} \quad (8)$$

as the set of the IDG where their power references have been set at the maximum or minimum values respectively. Therefore, the optimal power generation for each generator is given by equation [18]:

$$p_i^* = \begin{cases} p_{max,i} & \text{if } i \in \Omega_M \\ p_{r,i}^* & \text{if } i \notin \Omega_M \cup \Omega_m \\ p_{min,i} & \text{if } i \in \Omega_m \end{cases} \quad (9)$$

and consequently, the first-order optimality condition is given by [18]:

$$\lambda^* = \frac{p_d - p_{sat} + \sum_{i \notin \Omega_M \cup \Omega_m} \frac{\beta_i}{2\gamma_i}}{\sum_{i \notin \Omega_M \cup \Omega_m} \frac{1}{2\gamma_i}} \quad (10)$$

where:

$$p_{sat} = \sum_{i \in \Omega_M} p_{max,i} + \sum_{i \in \Omega_m} p_{min,i} \quad (11)$$

3. The Real Time Energy Management Strategy

In this section a novel real-time EMS is proposed for a PMG operating on island mode. Firstly, an estimation method for the real-time load demand measurement (p_d) is introduced. Given that in steady state $\sum_{i=1}^n p_i = p_d$, if the steady-state injected power measurement of each IDG is collected by the MGCC, then the power demand can be estimated as:

$$p_{d,m} = \sum_{i \in \mathcal{N}} p_{i,m} \quad (12)$$

where p_i^m is the instantaneous active power injected to the PMG by the i th IDG. Assuming a cooperative behavior and non-information restrictions between the prosumers, where the MGCC knows the cost function parameters of all IDGs (i.e., α_i , β_i , and γ_i for all $i \in \mathcal{N}$), a real-time strategy to solve the EDP in an islanded PMG is proposed according to the Cyber Physical model architecture shown in Figure 2. In this framework, the local measurements of injected active power from each IDG are sent to the MGCC to compute the load demand in real-time, using the centralized communication architecture shown in Figure 2.

The MGCC runs a dynamic algorithm described by (13) to find the optimal power reference allocation, which are tracked in by the IDG primary controllers. Thus, the MGCC computes the Lagrangian value λ in real-time according to the following continuous-time dynamics:

$$\dot{\lambda} = k \left(p_d^m - \sum_{i \in \mathcal{N}} p_{ref,i} \right) \quad (13)$$

where k is a control parameter, and $p_{ref,i} = p_i^*$, where p_i^* was defined in (9). Note that the continuous-time dynamic algorithm (13) allows the use of the Lyapunov stability analysis to determine convergence and optimality characteristics, and address the optimization problem from a

dynamic systems perspective [23]. These optimality and convergence properties are presented in the following section.

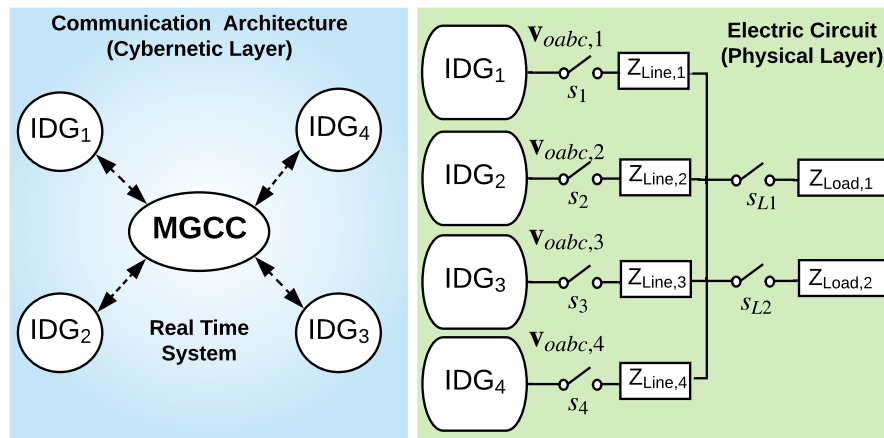


Figure 2. Cyber Physical Model of the PMG.

4. Optimality, Convergence and Frequency Regulation Properties of the Real Time EMS

The convergence and optimality properties of the algorithm (13) were proved for a grid connected case in the previous work [14]. In this work the proof is extended to the islanded operation case, following a similar sketch. For the sake of completeness the complete convergence and optimality properties and proofs are presented here.

4.1. Optimal Power References Allocation and Convergence

In order to prove that the steady state of the algorithm (13) corresponds with the optimal solution of the EDP, the following lemma is introduced.

Lemma 1. For $k > 0$, $\gamma_i > 0 \quad \forall i \in \mathcal{N}$, the dynamics described by (13) has an unique asymptotically stable equilibrium point given by:

$$\hat{\lambda} = \frac{\sum_{i \in \mathcal{N}} p_i - p_{sat} + \sum_{i \notin \Omega_M \cup \Omega_m} \frac{\beta_i}{2\gamma_i}}{\sum_{i \notin \Omega_M \cup \Omega_m} \frac{1}{2\gamma_i}} \quad (14)$$

Proof. From (13), $\dot{\lambda} = 0$ yields:

$$p_d^m = \sum_{i \in \mathcal{N}} p_{ref,i} = \sum_{i \in \mathcal{N}} p_i^* \quad (15)$$

Using (9), (15) can be rewritten as:

$$p_d^m = p_{sat} + \sum_{i \notin \Omega_M \cup \Omega_m} \left(\frac{\lambda - \beta_i}{2\gamma_i} \right) \quad (16)$$

Assuming that the real power demand is accurately estimated by the measured power generation (i.e., $p_d = p_d^m = \sum_{i \in \mathcal{N}} p_i^m$), we obtain the unique equilibrium point given by (14). Defining the variable $y = \lambda - \hat{\lambda}$, the dynamic system given in (13) can be expressed as $\dot{y} = -k \sum_{i=1}^N \frac{1}{2\gamma_i} y$. Note that this dynamic equation is nonlinear owing to the piecewise function given by (9). Therefore, assuming a quadratic Lyapunov function given by $V(y) = \frac{y^2}{2 \sum_{i \in \Omega_p} \frac{1}{2\gamma_i}}$, we obtain $\dot{V}(y) = -ky^2$. Given that $\frac{1}{2\gamma_i} > 0 \quad \forall i \in \mathcal{N}$, then for $k > 0$, $\dot{V}(y) < 0 \quad \forall x \neq 0$, and the equilibrium point $y = 0$, as well as, the unique equilibrium point of $\hat{\lambda}$ is globally asymptotically stable. \square

The optimality and convergence properties of the proposed real-time EMS are described in the next proposition.

Proposition 1. For $k > 0$, $\gamma_i > 0 \quad \forall i \in \mathcal{N}$, the power allocation given by the steady-state of the dynamic system (13) solves the EDP.

Proof. Given that the sum of a convex function is also a convex function, and the energy cost functions of the IDG given by (2) are convex, then the first-order optimality condition described in (10) is a necessary and sufficient condition to solve the EDP [22]. From the Lemma 1, the equilibrium point of the dynamic system (13) corresponds to the first-order optimality condition shown in (10), and it is globally asymptotically stable for $k > 0$ and $\gamma_i > 0 \quad \forall i \in \mathcal{N}$. \square

4.2. Frequency Regulation Property of the Real Time EMS

In this section, we show that the proposed real-time EMS performs implicitly as frequency regulation task, normally assigned to the secondary level of control in the conventional hierarchical control for microgrids [20]. Firstly, we assume that a conventional droop control strategy is implemented as primary controller. This control level is in charge of supplying the reference signals to the inner controller. With a proper inner controller tuning, which will be described on Section 5.1.2, each IDG can be represented by a Voltage Controlled Source (VCS) with a three-phase symmetric output voltage given by:

$$\mathbf{v}_{abc,i} = v_i \begin{bmatrix} \sin(\alpha_i) \\ \sin(\alpha_i - 120^\circ) \\ \sin(\alpha_i + 120^\circ) \end{bmatrix}$$

where the variables $v_i \in \mathbb{R}_{\geq 0}$, and $\alpha_i \in \mathbb{S}$ are defined by the primary controller as $\dot{\alpha}_i = u_i^\alpha$, and $v_i = u_i^v$, according to the hierarchical microgrid control approach [20]. Note that $\dot{\alpha}_i = \omega_i$ and the phase α_i and output voltage regulation are assumed as instantaneous [24,25]. Based on the assumption of a dependency between the active and reactive power with the frequency and the amplitude voltage, the reference signal generator variables u_i^α and u_i^v are defined as [24]:

$$u_i^v = v_n - n_i \cdot q_{m,i} \quad (17)$$

$$u_i^\alpha = \omega_i = \omega_n - m_i (p_{m,i} - p_{\text{ref},i}) \quad (18)$$

where ω_n and v_n are the nominal angular frequency and voltage of the IDG respectively, n_i and m_i are the droop coefficients, $p_{m,i}$ and $q_{m,i}$ are the measured active and reactive output power from the i th generator, and p_i^* is the active power reference calculated by the EMS. The power measurement is typically performed by a first order low pass filter described as [26]:

$$\tau_m \dot{p}_{m,i} = p_i - p_{m,i} \quad (19)$$

$$\tau_m \dot{q}_{m,i} = q_i - p_{m,i} \quad (20)$$

where p_i and q_i are the instantaneous active and reactive power values calculated using the instantaneous power p-q theory as [21]:

$$p_i = v_{\alpha,i} i_{\alpha,i} + v_{\beta,i} i_{\beta,i} \quad (21)$$

$$q_i = v_{\alpha,i} i_{\beta,i} - v_{\beta,i} i_{\alpha,i} \quad (22)$$

and $v_{\alpha,i}$, $i_{\alpha,i}$, $v_{\beta,i}$, and $i_{\beta,i}$ are the synchronous reference frame voltage and current signals, which are obtained applying the Clark transformation to the three phase measurements signals of voltage and currents ($v_{abc,i}$ and $i_{abc,i}$). As a quality standard requirement, the frequency and voltage magnitude must be regulated strictly in the PMG, and the droop constants must be limited by $m_i = \frac{\Delta\omega}{p_{\text{max}}}$ and

$n_i = \frac{\Delta v}{q_{max}}$, where p_{max} and q_{max} are the maximum active and reactive power which can be delivered and Δw and Δv are the the maximum allowed frequency and magnitude voltage [26].

Proposition 2. For $k > 0$, $m_i = m \in \mathbb{R}_{\geq 0} \quad \forall i \in \mathcal{N}$, the power allocation given by the real-time EMS (13) and the conventional droop primary controller (18) leads to the frequency steady-state:

$$\omega_i^{ss} = \omega_n \quad \forall i \in \mathcal{N} \quad (23)$$

where ω_i^{ss} denotes the frequency output steady-state of the i th IDG.

Proof. From (19), in steady-state $\dot{p}_{m,i} = 0$, and $p_i^{ss} = p_{m,i}^{ss}$ and $\sum_{i \in \mathcal{N}} p_{m,i}^{ss} = \sum_{i \in \mathcal{N}} p_i^{ss}$, where the super-index ss denotes the steady-state values. Summing over all n on both sides of (18), and owing to the condition $m_i = m \in \mathbb{R}_{\geq 0} \quad \forall i \in \mathcal{N}$, we obtain:

$$\sum_{i \in \mathcal{N}} (\omega_i - \omega_n) = -m \sum_{i \in \mathcal{N}} (p_{m,i} - p_{ref,i}) \quad (24)$$

From (13), in steady-sate we have $\dot{\lambda} = 0$ and

$$\sum_{i \in \mathcal{N}} p_{m,i}^{ss} = \sum_{i \in \mathcal{N}} p_{ref,i}^{ss} = \sum_{i \in \mathcal{N}} p_i^{ss} \quad (25)$$

which leads to $\sum_{i \in \mathcal{N}} (\omega_i^{ss} - \omega_n) = 0$, and (23). \square

Remark 1 (Reduction cost and complexity of the secondary control implementation). Note that the frequency regulation property described in Proposition 2 implies that the control objective of the secondary controller in the hierarchical microgrid control approach [27] can be achieved by the tertiary level controller implementing the proposed real-time EMS, reducing the communications requirements and complexity of the secondary control implementation. Similar results have been reported recently in the literature without experimental demonstrations [28].

In order to give a general view of the control strategy described previously, the proposed EMS has been represented by the concurrent flow diagram shown in Figure 3. Note that the processes on the IDGs and the MGCC occurs concurrently and in real-time.

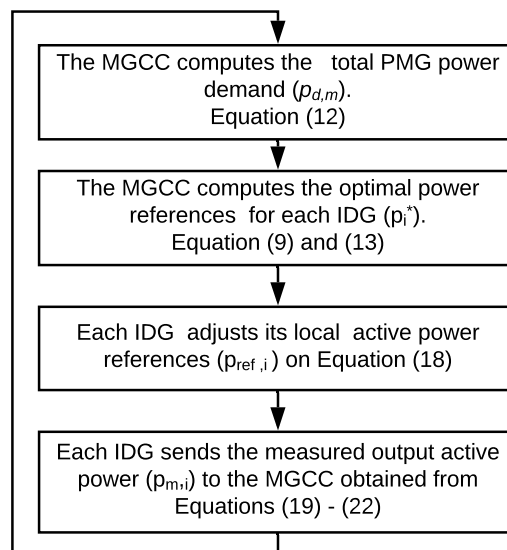


Figure 3. Flow diagram of the proposed EMS.

5. Results

5.1. Inverter-Based Distributed Generator Implementation

The control block diagram of an IDG is shown in Figure 4, where the generator has two main components: a physical power system and a control system. The physical power system consists of a three-phase DC–AC converter, an LC filter and a Pulsewidth Modulation (PWM) block. On the other hand, the control system is classified in two main control levels, namely: primary controller and inner controller. The instantaneous values of inductor currents (i_{fab}), and capacitor voltages (v_{oabc}) are measured and transformed to $\alpha\beta$ coordinates using the Clarke's transformation [21]. These signals are used like control inputs to a double loop voltage inner controller.

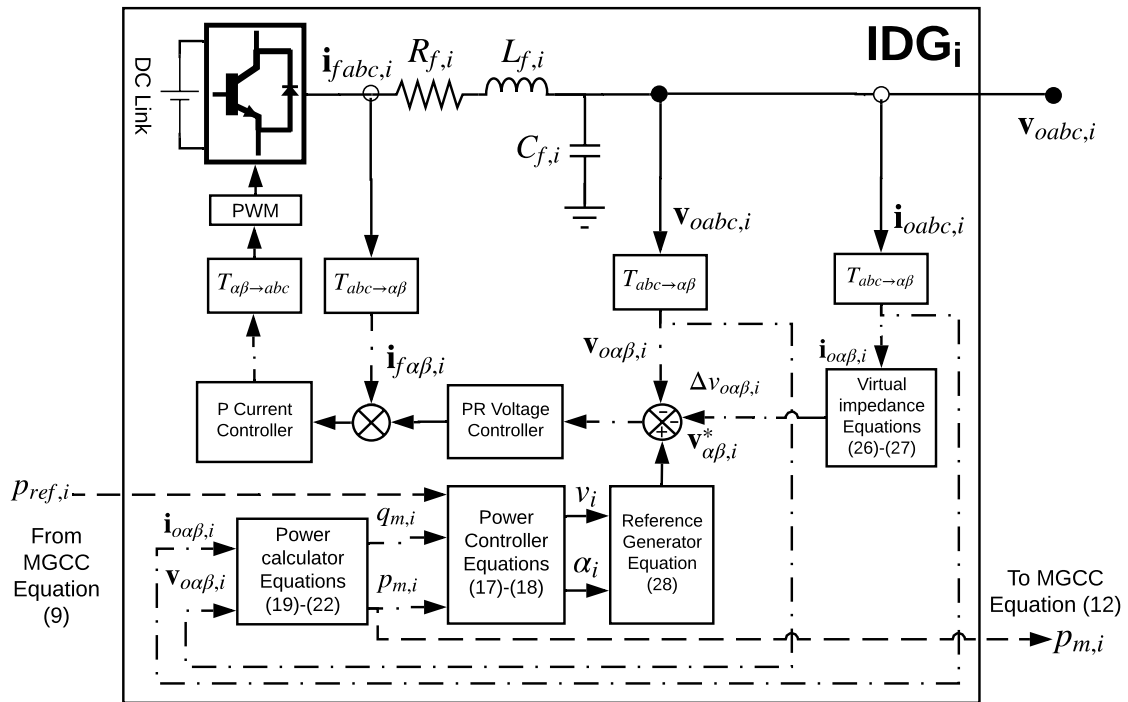


Figure 4. Inverter-based Distributed Generator implementation.

5.1.1. Power Controller Implementation

The power controller is implemented based on the conventional droop controller described on Section 4.2, Equations (17)–(22) and this is shown in Figure 4. Additionally, each IDG local controller implements a virtual impedance loop, where a dominant output impedance $z_v = r_v + jx_v \in \mathbb{C}$ is emulated, where $r_v \in \mathbb{R}_{>0}$ and $x_v \in \mathbb{R}_{>0}$ are the virtual resistance and reactance parameters. The equivalent line impedance parameters can be defined as $z_{e,i} = r_{e,i} + jx_{e,i}$, where $r_{e,i} = r_v + r_{l,i}$ and $x_{e,i} = x_v + x_{l,i}$. The virtual loop impedance is implemented in the stationary reference frame ($\alpha\beta$ coordinates) as [19]:

$$\Delta v_{\alpha,i} = r_v i_{o\alpha,i} - x_v i_{o\beta,i} \quad (26)$$

$$\Delta v_{\beta,i} = r_v i_{o\beta,i} + x_v i_{o\alpha,i} \quad (27)$$

5.1.2. Inner Controller Implementation

The voltage double loop inner controller uses a proportional current controller and a Proportional Resonant (PR)-voltage controller in $\alpha\beta$ reference frame to track a $\alpha\beta$ reference signals [19], which are

generated by the “Reference Generator” block. The voltage reference generator block produces the local reference voltage as:

$$v_{\alpha,i}^* = v_i \sin(\alpha_i), \quad v_{\beta,i}^* = v_i \cos(\alpha_i) \quad (28)$$

where $v_i \in \mathbb{R}_{>0}$ is the amplitude voltage reference value and $\alpha_i = \omega_i t$. In order to simplify the notation, the vectors $\mathbf{v}_{\alpha\beta,i} = [v_{\alpha,i}, v_{\beta,i}]^T$, $\mathbf{v}_{o\alpha\beta,i} = [v_{o\alpha,i}, v_{o\beta,i}]^T$ are introduced. The voltage reference signal ($\mathbf{v}_{\alpha\beta,i}^*$) is used as voltage reference input for a Proportional-Resonant (PR) inner controller, which is based on a PR-voltage loop and a proportional current loop, which is selected owing to its zero steady state tracking error characteristics and simple implementation [19]. A general scheme the inner controller is shown in Figure 5, which is tuned such that it achieves a fast voltage reference tracking, and $\mathbf{v}_{o\alpha\beta,i} \rightarrow \mathbf{v}_{r\alpha\beta,i}^*$ owing to the fast inner control response.

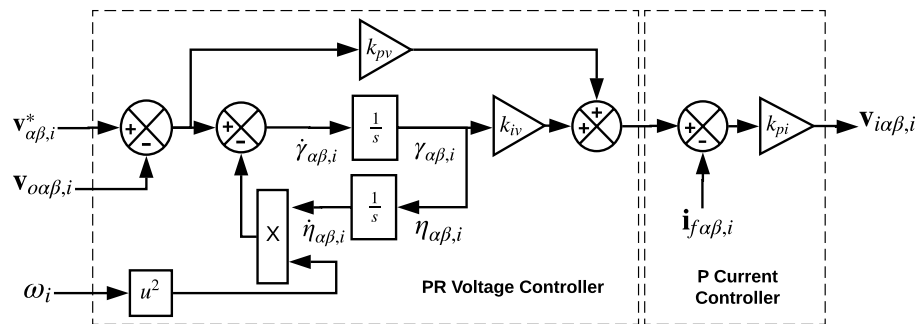


Figure 5. PR-P Inner Controller.

5.2. Experimental Setup

In this section, we validate the effectiveness and performance of the proposed EMS via an experimental study case based on the Cyber Physical System (CPS) model shown in Figure 2. Both the communication architecture and the electric system configuration of the tested network is presented in Figure 2, which have the associated parameters described on Table 1. This PMG architecture is implemented in an experimental set-up at the Aalborg Intelligent Microgrids Laboratory [29] shown in Figure 6. The experimental setup consists of four IDGs, implemented with commercial Danfoss 2.2 kW inverters and LC output filters, which emulate an islanded PMG with mismatched line feeder parameters. The measurements are performed using LEM sensors, and the EMS algorithm is implemented on the real-time platform dSPACE1106 board, which provides computing power for the real-time system and also functions as an interface with the host PC and with the input/output boards. The control models are developed in Matlab/Simulink and compiled in C++, and run on the DS1006 processor board of dSPACE real-time control platform. The communication links were simulated on Simulink and the dSPACE real-time platform with the time step $t_{com} = 100$ ms. The system specification for hardware implementation is listed in Table 1.

To conduct the experiments it is assumed that all the time there is enough power availability to supply the load demand. It is:

$$p_d < \sum_{i=1}^n p_{max,i}, \quad \forall t > 0 \quad (29)$$

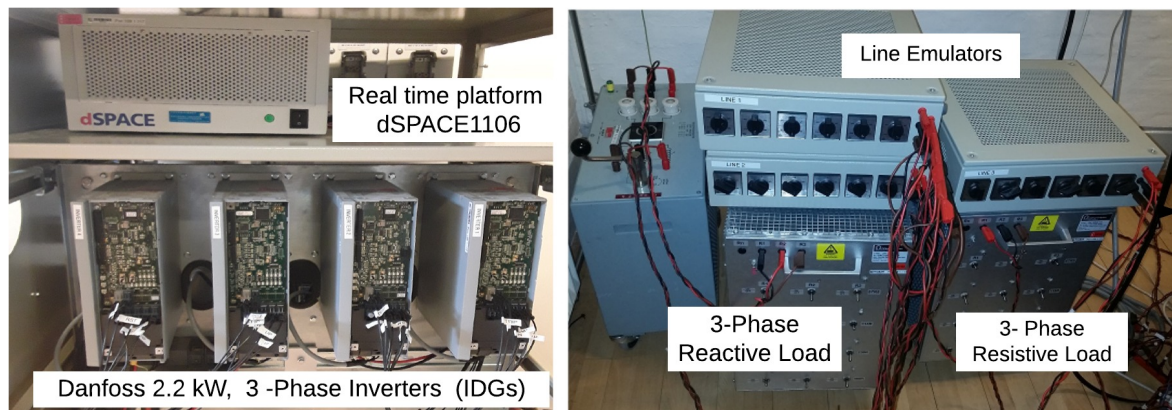
To evaluate the performance of the EMS different connection and disconnection events are forced. Initially all the IDG are connected to the PMG after an earlier synchronization process. At 0s, an active load ($Z_{load,1}$) is connected to the PMG closing the relay s_{L1} . Next at $t = 4, 5$ s, the relay s_{L2} is closed and the reactive load $Z_{load,2}$ is connected to the PMG. At $t = 10, 5$ s the third IDG is disconnected suddenly. In a similar manner, at 16s the forth IDG is disconnected. The IDG parameters are shown in Table 2 (cost coefficients and output power limits).

Table 1. Microgrid Setup Parameters.

System Parameters	Values
Nominal amplitude voltage (v_n)	311 V
Nominal frequency (f_n)	50 Hz
Filter Inductance ($L_{f,i}$)	1.8 mH
Capacitance Filter ($C_{f,i}$)	9 μ F
Filter resistor ($R_{f,i}$)	0.1 Ω
DC link voltage (V_{DC})	1000 V
Danfoss Converter FC302	2.2 kW
Proportional voltage controller gain (k_{pV})	0.04
Resonant voltage controller gain (k_{iv})	94
Current controller gain (k_{pi})	0.9
Frequency droop controller gain 1 and 2 (m_1, m_2)	0.5×10^{-4}
Frequency droop controller gain 3 and 4 (m_3, m_4)	1×10^{-4}
Voltage droop controller gain (n_i)	0.01
Line impedance IDG_1 ($Z_{Line,1}$)	$0.39 \Omega + j0.50 \Omega$
Line impedance IDG_2 ($Z_{Line,2}$)	$0.68 \Omega + j0.60 \Omega$
Line impedance IDG_3 ($Z_{Line,3}$)	$0.68 \Omega + j0.50 \Omega$
Line impedance IDG_4 ($Z_{Line,4}$)	$0.22 \Omega + j0.79 \Omega$
Load 1 ($Z_{Load,1}$)	58.9 Ω
Load 2 ($Z_{Load,2}$)	$117 \Omega + j50 \Omega$

Table 2. Inverter based distributed generators parameters.

i	α_i (\$/W)	β_i (\$/W ²)	p_i^{max} (W)	p_i^{min} (W)
1	0.06	0.5	2200	−2200
2	0.03	0.25	2200	−2200
3	0.04	0.3	1000	−1000
4	0.005	0	1000	0

**Figure 6.** Experiment setup.

5.3. Experimental Results with a Conventional Power Sharing Droop Control

The power sharing performance for the conventional droop controller is shown in Figure 7. As we can see, the active power demand is shared between the IDGs, proportionally to their power ratings and a stable performance is achieved under sudden loads and IDGs connection and disconnection. However, the power references allocation do not follow the optimal values (i.e., p_1^*, \dots, p_4^*) computed based on the Equation (9). Additionally, Figure 8 shows that the IDG frequency outputs deviate from the nominal value.

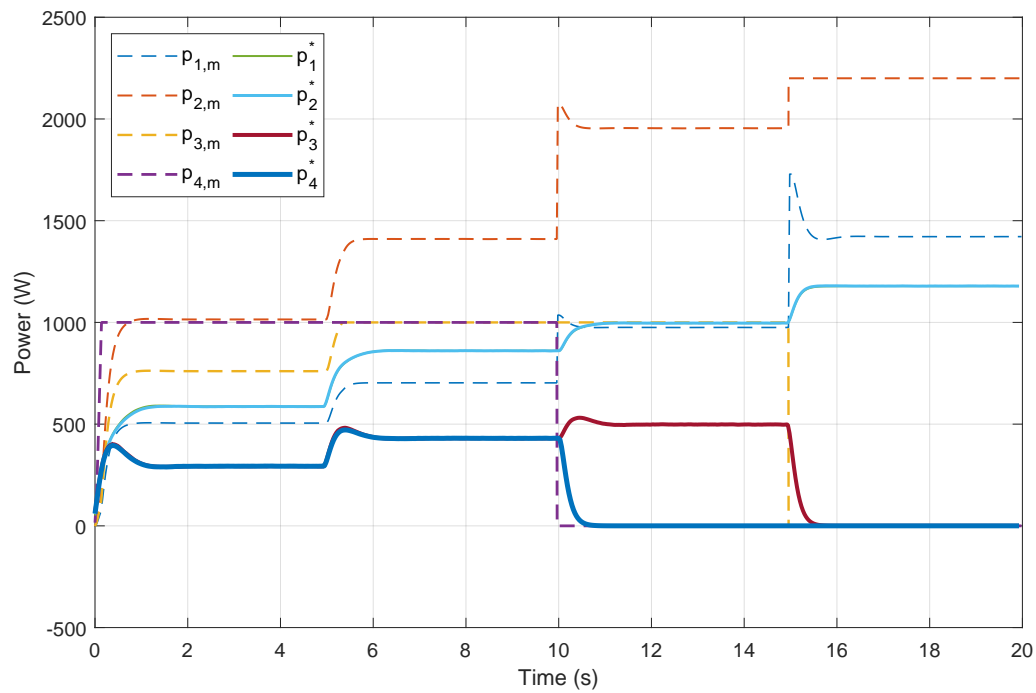


Figure 7. Conventional droop control strategy performance: Active power sharing. The conventional droop control strategy can achieve proportional power sharing without any minimum/maximum capacity restriction violation. However, the injected power steady-state values ($p_{1,m}, \dots, p_{4,m}$) do not track the optimal power references (p_1^*, \dots, p_4^*) that lead to a real-time optimal economic operation. The optimal references have been computed in real-time using the Equations (9)–(11).

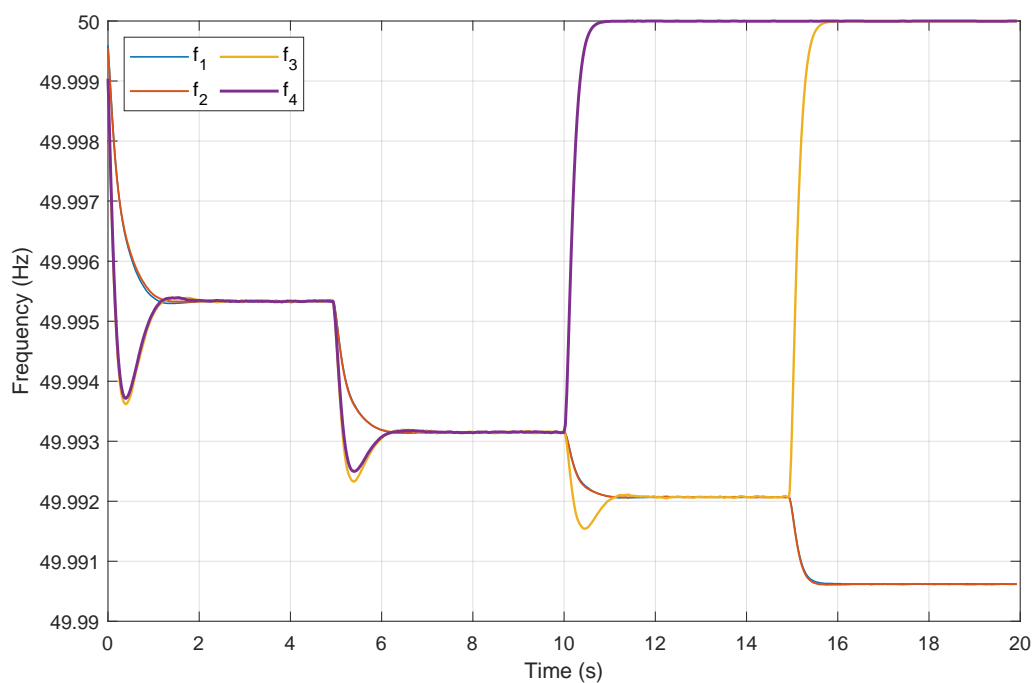


Figure 8. Conventional droop control strategy performance: Frequency regulation. In order to response to load and generation changes and guarantee proportional power sharing between IDGs, the frequency value deviates from the nominal value (50 Hz) proportionally to the active power demand. That means that using this conventional technique exists an implicit trade-off between frequency regulation and power sharing control.

5.4. Experimental Results with the Real-Time Energy Management Strategy

The proposed real-time EMS proposed in the dynamic algorithm (13) is implemented in Simulink/Dspace environment and download to the DS1006 processor board. The power generation of each IDG is measured in real-time and sent to the MGCC to compute the total load demand (p_d) based on Equation (12). The experimental results using the real-time EMS are shown in Figures 9–11. In Figure 9, dot lines correspond to the power references computed by the EMS (i.e., p_1^*, \dots, p_4^*). These power references are computed by the dynamic equation described on the (13) and the algebraic Equation (9), which are implemented on Matlab/Simulink, automatic compiled in C++ and run on the real-time platform dSPACE1106. As we can see, the real-time measured generated power is following the optimal references with very low steady state error. On the other hand, the frequency regulation performance is shown in Figure 10. An Integral Quadratic Error (IQE) index is used to evaluate the frequency regulation performance, which is given by:

$$IQE_i = \int_{t_0}^{t_{end}} (f_i - f_n)^2 \quad (30)$$

A performance comparison of the conventional droop control strategy and the proposed real-time EMS is presented in Table 3, where the IQE index for the 20s study case are included. As we can see, the frequency regulation performance of the real-time EMS is better than the conventional power sharing strategy for all the IDGs.

Finally, the voltage profile results are shown in Figure 11. We can see that the direct components of the output voltage of each IDG ($v_{od1,m}, v_{od2,m}, v_{od3,m}, v_{od4,m}$) do not violate the voltage limits restrictions (v_{max}, v_{min}) in any time of the test.

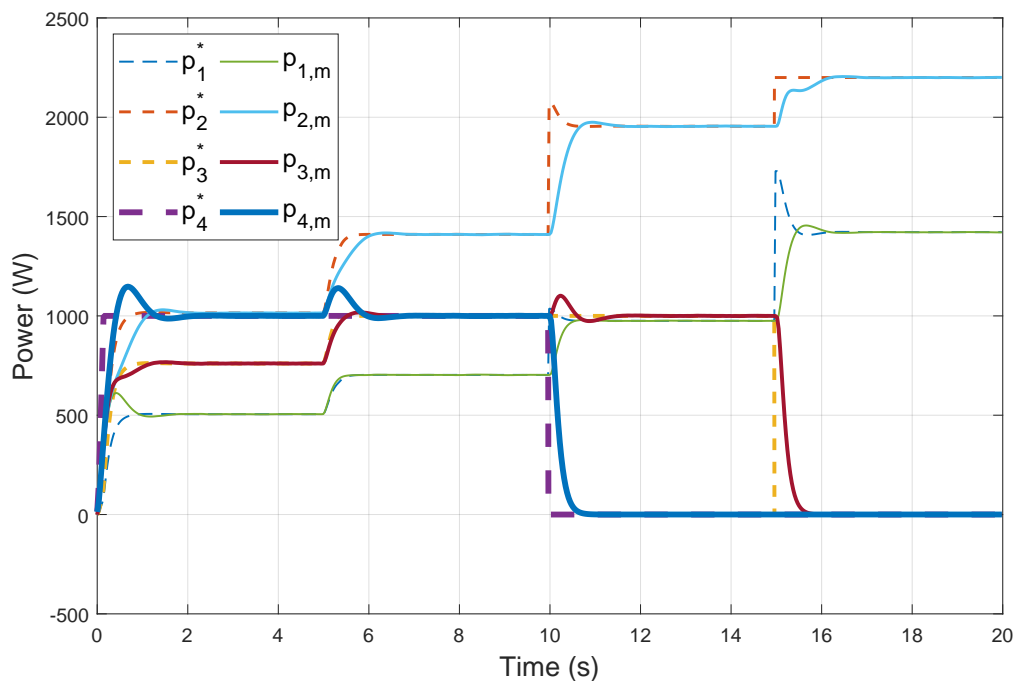


Figure 9. Optimal power allocation and tracking with the real-time EMS. As it was shown by Proposition 1, running the dynamic algorithm (13) and computing in real-time power references based on the Equations (9)–(11), the injected power achieve a proper tracking of the optimal power references (p_1^*, \dots, p_4^*). The inner controller shows an adequate tracking performance that leads to optimal economic operation in real-time.

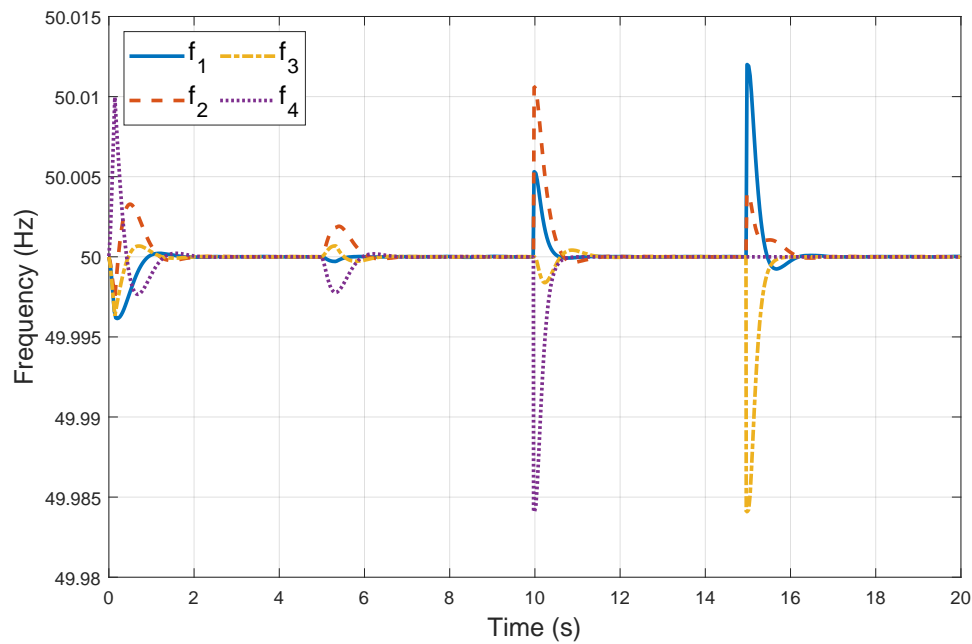


Figure 10. Frequency regulation performance with the real-time EMS. Unlike to the conventional droop control results (see Figure 8), the proposed real-time EMS achieves a proper frequency regulation performance as it was shown in the Proposition 2.

Table 3. Frequency regulation performance: IQE index.

IQE_i	1	2	3	4
Conventional Droop Control	1.069	1.069	0.6756	0.359
Real Time EMS	0.035	0.035	0.0479	0.056

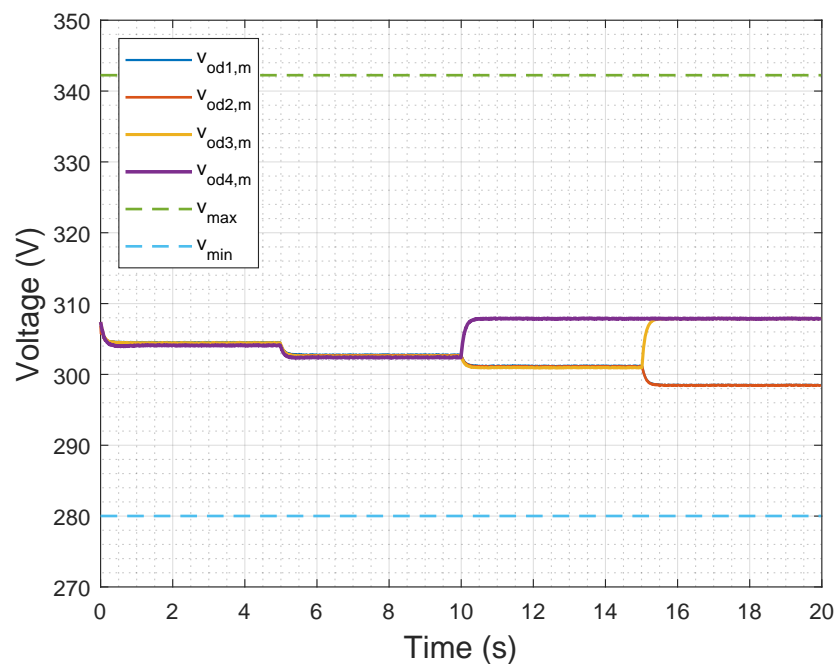


Figure 11. Voltage profile with the real-time EMS. The direct components of the output voltage of each IDG ($v_{od1,m}$, $v_{od2,m}$, $v_{od3,m}$, $v_{od4,m}$) are shown in this figure. The voltage limits restrictions of $\pm 10\%$ of the nominal voltage amplitude (v_{max} , v_{min}) are not violated in any time of the test.

6. Conclusions

In this paper, an experimental demonstration of a novel real-time energy management strategy for islanded Prosumer Microgrid (PMG) has been presented. The strategy solves the economic dispatch problem on the PMG scenario using a simple real-time dynamic algorithm without the requirement of offline optimization. The convergence and optimality properties of the strategy are demonstrated, and the effectiveness and compatibility with the inner and primary controllers are validated in an experimental study case with four distributed generators, which is implemented at the Aalborg Intelligent Microgrids Laboratory. According to the results, the proposed EMS shows an adequate stability performance in the optimal power reference tracking under sudden load changes and IDG disconnections. Additionally, a performance comparison with the conventional droop control strategy has been carried out, where the experimental results show a better performance on power tracking and frequency regulation when the proposed real-time EMS is implemented.

As future work, distributed real-time energy management strategies can be addressed in order to reduce the communication infrastructure cost and reduce the vulnerability of the system to single point failures. Additionally, sharing information restrictions and non-cooperative prosumers considering smart loads and PV-systems can be included in future test scenarios.

Author Contributions: Conceptualization, Methodology, Software, Validation and Formal Analysis, Investigation C.A.M.; Resources H.R.P., J.C.V., and J.M.G.; Writing—Original Draft Preparation, C.A.M.; Writing—Review and Editing, C.A.M., H.R.P., and Q.Z.; Visualization, C.A.M.; Supervision, H.R.P., J.C.V. and J.M.G.; Project Administration, H.R.P.; Funding Acquisition, H.R.P., J.C.V. and J.M.G.

Funding: This research was funded by the University of New South Wales, Tuition Fee Scholarship (RSRE7059 and RSRE7060) and the “Departamento Administrativo de Ciencia, Tecnología e Innovación” Scholarship Program No. 679-2014.

Conflicts of Interest: The authors declare no conflict of interest. The founding sponsors had no role in the design of the study; in the collection, analyses, or interpretation of data; in the writing of the manuscript, and in the decision to publish the results

Abbreviations

The following abbreviations are used in this manuscript:

PMG	Prosumer Microgrid
IDG	Inverter based Distributed Generator
MGCC	Microgrid Central Controller
BESS	Battery Energy Storage System
EMS	Energy Management System
RES	Renewable Energy Source
EDP	Economic Dispatch Problem
PV	Photovoltaic System
MPPT	Maximum Power Point Tracking
PWM	Pulsewidth Modulation
PR	Proportional Resonant
VCS	Voltage Controlled Source
CPS	Cyber Physical System
IQE	Integral Quadratic Error

References

1. Chapman, A.J.; McLellan, B.; Tezuka, T. Residential solar PV policy: An analysis of impacts, successes and failures in the Australian case. *Renew. Energy* **2016**, *86*, 1265–1279. [[CrossRef](#)]
2. Parag, Y.; Sovacool, B.K. Electricity market design for the prosumer era. *Nat. Energy* **2016**, *1*, 16032. [[CrossRef](#)]
3. Zubietta, L.E. Are Microgrids the Future of Energy?: DC Microgrids from Concept to Demonstration to Deployment. *IEEE Electr. Mag.* **2016**, *4*, 37–44. [[CrossRef](#)]

4. Zhou, K.; Yang, S.; Shao, Z. Energy Internet: The business perspective. *Appl. Energy* **2016**, *178*, 212–222. [[CrossRef](#)]
5. Olivares, D.E.; Cañizares, C.A.; Kazerani, M. A Centralized Energy Management System for Isolated Microgrids. *IEEE Trans. Smart Grid* **2014**, *5*, 1864–1875. [[CrossRef](#)]
6. Manz, D.; Walling, R.; Miller, N.; Larose, B.; D'Aquila, R.; Daryanian, B. The grid of the future: Ten trends that will shape the grid over the next decade. *IEEE Power Energy Mag.* **2014**, *12*, 26–36. [[CrossRef](#)]
7. Luna, A.; Meng, L.; Aldana, N.D.; Graells, M.; Vasquez, J.; Guerrero, J. Online Energy Management Systems for Microgrids: Experimental Validation and Assessment Framework. *IEEE Trans. Power Electron.* **2017**, *33*, 2201–2215. [[CrossRef](#)]
8. Macana, C.; Abdou, A.; Pota, H.; Guerrero, J.; Vasquez, J. Cyber Physical Energy Systems Modules for Power Sharing Controllers in Inverter Based Microgrids. *Inventions* **2018**, *3*, 66. [[CrossRef](#)]
9. Macana, C.A.; Pota, H. New trends of reactive power sharing control for islanded microgrids: A cyber-physical review. In Proceedings of the 2016 IEEE Innovative Smart Grid Technologies—Asia (ISGT-Asia), Melbourne, Australia, 28 November–1 December 2016; pp. 353–358. [[CrossRef](#)]
10. Kaur, A.; Kaushal, J.; Basak, P. A review on microgrid central controller. *Renew. Sustain. Energy Rev.* **2016**, *55*, 338–345. [[CrossRef](#)]
11. Di Fazio, A.; Russo, M.; De Santis, M. Zoning Evaluation for Voltage Optimization in Distribution Networks with Distributed Energy Resources. *Energies* **2019**, *12*, 390. [[CrossRef](#)]
12. Mojica-Nava, E.; Macana, C.A.; Quijano, N. Dynamic Population Games for Optimal Dispatch on Hierarchical Microgrid Control. *IEEE Trans. Syst. Man Cybern. Syst.* **2014**, *44*, 306–317. [[CrossRef](#)]
13. Milano, F.; Dorfler, F.; Hug, G.; Hill, D.J.; Verbic, G. Foundations and Challenges of Low-Inertia Systems (Invited Paper). In Proceedings of the 2018 Power Systems Computation Conference (PSCC), Dublin, Ireland, 11–15 June 2018; pp. 1–25. [[CrossRef](#)]
14. Macana, C.A.; Mohiuddin, S.M.; Pota, H.R.; Mahmud, M. Online energy management strategy for islanded microgrids with feedback linearizing inner controllers. In Proceedings of the 2017 IEEE Innovative Smart Grid Technologies—Asia (ISGT-Asia), Auckland, New Zealand, 4–7 December 2017; pp. 1–6. [[CrossRef](#)]
15. Han, Y.; Li, H.; Shen, P.; Coelho, E.A.A.; Guerrero, J.M. Review of Active and Reactive Power Sharing Strategies in Hierarchical Controlled Microgrids. *IEEE Trans. Power Electron.* **2017**, *32*, 2427–2451. [[CrossRef](#)]
16. Meng, L.; Sanseverino, E.R.; Luna, A.; Dragicevic, T.; Vasquez, J.C.; Guerrero, J.M. Microgrid supervisory controllers and energy management systems: A literature review. *Renew. Sustain. Energy Rev.* **2016**, *60*, 1263–1273. [[CrossRef](#)]
17. Nwulu, N.I.; Xia, X. Optimal dispatch for a microgrid incorporating renewables and demand response. *Renew. Energy* **2017**, *101*, 16–28. [[CrossRef](#)]
18. Chen, G.; Lewis, F.L.; Feng, E.N.; Song, Y. Distributed Optimal Active Power Control of Multiple Generation Systems. *IEEE Trans. Ind. Electron.* **2015**, *62*, 7079–7090. [[CrossRef](#)]
19. Vasquez, J.C.; Guerrero, J.M.; Savaghebi, M.; Eloy-Garcia, J.; Teodorescu, R. Modeling, Analysis, and Design of Stationary-Reference-Frame Droop-Controlled Parallel Three-Phase Voltage Source Inverters. *IEEE Trans. Ind. Electron.* **2013**, *60*, 1271–1280. [[CrossRef](#)]
20. Guerrero, J.M.; Chandorkar, M.; Lee, T.L.; Loh, P.C. Advanced Control Architectures for Intelligent Microgrids. Part I: Decentralized and Hierarchical Control. *IEEE Trans. Ind. Electron.* **2013**, *60*, 1254–1262. [[CrossRef](#)]
21. Czarnecki, L. Instantaneous Reactive Power p-q Theory and Power Properties of Three-Phase Systems. *IEEE Trans. Power Deliv.* **2006**, *21*, 362–367. [[CrossRef](#)]
22. Boyd, S.; Vandenberghe, L. *Convex Optimization*; Cambridge University Press: New York, NY, USA, 2004. [[CrossRef](#)]
23. Wang, J.; Elia, N. A control perspective for centralized and distributed convex optimization. In Proceedings of the 2011 50th IEEE Conference on Decision and Control and European Control Conference, Orlando, FL, USA, 12–15 December 2011; pp. 3800–3805. [[CrossRef](#)]
24. Schiffer, J.; Ortega, R.; Astolfi, A.; Raisch, J.; Sezi, T. Conditions for stability of droop-controlled inverter-based microgrids. *Automatica* **2014**, *50*, 2457–2469. [[CrossRef](#)]
25. Simpson-Porco, J.W.; Dorfler, F.; Bullo, F. Synchronization and power sharing for droop-controlled inverters in islanded microgrids. *Automatica* **2013**, *49*, 2603–2611. [[CrossRef](#)]

26. He, J.; Li, Y.W.; Guerrero, J.M.; Blaabjerg, F.; Vasquez, J.C. An Islanding Microgrid Power Sharing Approach Using Enhanced Virtual Impedance Control Scheme. *IEEE Trans. Power Electron.* **2013**, *28*, 5272–5282. [[CrossRef](#)]
27. Lu, X.; Yu, X.; Lai, J.; Guerrero, J.M.; Zhou, H. Distributed Secondary Voltage and Frequency Control for Islanded Microgrids With Uncertain Communication Links. *IEEE Trans. Ind. Inform.* **2017**, *13*, 448–460. [[CrossRef](#)]
28. Dörfler, F.; Simpson-Porco, J.W.; Bullo, F. Breaking the Hierarchy: Distributed Control and Economic Optimality in Microgrids. *IEEE Trans. Control Netw. Syst.* **2016**, *3*, 241–253. [[CrossRef](#)]
29. Meng, L.; Luna, A.; Diaz, E.; Sun, B.; Dragicevic, T.; Savaghebi, M.; Vasquez, J.; Guerrero, J.; Graells, M. Flexible System Integration and Advanced Hierarchical Control Architectures in the Microgrid Research Laboratory of Aalborg University. *IEEE Trans. Ind. Appl.* **2015**, *52*, 1736–1749. [[CrossRef](#)]



© 2019 by the authors. Licensee MDPI, Basel, Switzerland. This article is an open access article distributed under the terms and conditions of the Creative Commons Attribution (CC BY) license (<http://creativecommons.org/licenses/by/4.0/>).